Eur. Phys. J. A **23**, 481–490 (2005)
DOI 10.1140/epja/i2004-10112-y

THE EUROPEAN PHYSICAL JOURNAL A

# The $\beta^-$-decay of $^{147}$Cs to $^{147}$Ba

A. Syntfeld[1,2,a], H. Mach[3], W. Kurcewicz[2], B. Fogelberg[3], N. Amzal[4,b], J. Galy[3,c], K. Gulda[2,d], A. Korgul[2], A. Lindroth[3,e], W.A. Płóciennik[5], M. Sanchez-Vega[3,f], and W. Urban[2]

[1] Department of Detectors and Nuclear Electronics, Sołtan Institute for Nuclear Studies, 05-400 Świerk, Poland
[2] Institute of Experimental Physics, Warsaw University, Hoża 69, 00-681 Warsaw, Poland
[3] Department of Radiation Sciences, Uppsala University, 611 82 Nyköping, Sweden
[4] Oliver Lodge Laboratory, University of Liverpool, Liverpool, L69 3BX, UK
[5] Department of Nuclear Spectroscopy, Sołtan Institute for Nuclear Studies, 05-400 Świerk, Poland

Received: 23 August 2004 / Revised version: 18 November 2004 /
Published online: 18 January 2005 – 
Communicated by D. Schwalm

**Abstract.** The $\beta^-$-decay of $^{147}$Cs to $^{147}$Ba has been studied by means of $\gamma$- and X-ray spectroscopy. A new level scheme of $^{147}$Ba is significantly modified and extended in comparison to the one previously reported. The Advanced Time-Delayed $\beta\gamma\gamma$(t) method has been applied to measure half-lives of the 46.2 and 85.4 keV levels in $^{147}$Ba yielding $T_{1/2}$ of 510(80) ps and 370(100) ps, respectively. The lifetime results combined with the deduced internal conversion coefficients allowed to assign $M1$ multipolarity to three $\gamma$ transitions. The $B(M1)$ values obtained for the 39.2, 46.2 and 85.4 keV transitions range from 0.017 to 0.043 W.u. and represent typical $B(M1)$ strength in the Ba-Er region. Model calculations using a shell correction approach with the axially deformed Woods-Saxon potential predict for $^{147}$Ba an octupole deformed ground state with $\beta_3 = 0.11$.

**PACS.** 27.60.+j $90 \leq A \leq 149$ – 29.30.Kv X- and $\gamma$-ray spectroscopy – 21.10.Tg Lifetimes – 21.10.Ky Electromagnetic moments

## 1 Introduction

The region of neutron-rich Ba nuclei is known to exhibit strong octupole correlations. About 20 years ago, theoretical calculations performed by Nazarewicz *et al.* [1] predicted a region of octupole deformation around $^{146}$Ba, at $Z \simeq 56$, $N \simeq 90$. The neutron and proton orbitals involved in this region which favor octupole collectivity are those with stretched $\Delta l, \Delta j = 3$ coupling, thus $\nu i_{13/2}$-$\nu f_{7/2}$ and $\pi h_{11/2}$-$\pi d_{5/2}$. Following the model predictions, Phillips *et al.* [2] reported that the level patterns of $^{144}$Ba and $^{146}$Ba are similar to the rotational bands in reflection-asymmetric molecules or to those observed in light actinides (see also [3]). Along with enhanced $B(E1)$ rates in $^{144}$Ba, these findings have suggested that octupole deformation exists in these nuclei at moderate spins. Further experimental [4] and theoretical [5] studies in the even-even Ba region have shown that octupole correlations are more pronounced in $^{144}$Ba due to shell effects. In odd-$A$ bariums, the $^{145}$Ba isotope was predicted [6, 7] to be a good candidate to exhibit stable octupole deformation. However, no experimental evidence for strong octupole collectivity has been reported for this nucleus. A well-developed alternating-parity band, characteristic of a reflection-asymmetric shape of a nucleus, was only observed in $^{143}$Ba in the spontaneous-fission studies of $^{242}$Pu and $^{252}$Cf [8] as well as $^{248}$Cm [9]. The most recent results on $^{141}$Cs and $^{143}$Cs [10] indicate much weaker octupole correlations in these nuclei than observed in the corresponding even-even Ba isotones.

The aim of this work was to study the structure of the neutron-rich $^{147}$Ba nucleus by means of $\gamma$- and X-ray spectroscopy and level lifetime measurements. The measurements were performed at the OSIRIS facility in Studsvik, Sweden. They were part of wider systematic studies of octupole correlations in the Ba-Nd region carried out by

[a] e-mail: syntfeld@ipj.gov.pl
[b] *Present address*: School of ICT - EEP Division, University of Paisley, High Street PA1 2BE, Paisley, Scotland, UK.
[c] *Present address*: the European Commission, Joint Research Center, Institute for Transuranium, Postfach 2340, D-76125 Karlsruhe, Germany.
[d] *Present address*: Warsaw University, University Technology Transfer Centre, Zwirki i Wigury 93, 02-093 Warsaw, Poland, and Ministry of Economy and Labour, Department of Innovation, Pl. Trzech Krzyzy 3/5, 00-507 Warsaw, Poland.
[e] *Present address*: Instituut voor Kern- en Stralingsfysica, University of Leuven, B-3001 Leuven, Belgium.
[f] *Present address*: Kernfysisch Versneller Instituut, Zernikelaan 25, NL-9747 AA Groningen, The Netherlands.

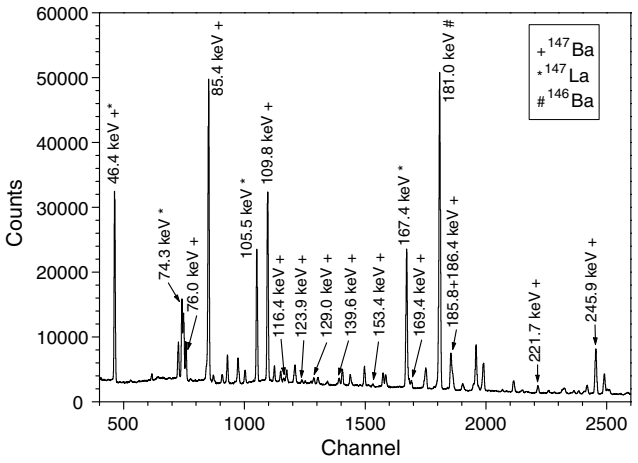


**Fig. 1.** A portion of the $\gamma$-ray singles spectrum recorded in the LOAX detector in the first time group of the MSS measurement (see text for details). Besides $\gamma$-lines from $^{147}$Ba, the strongest impurity transitions from $^{147}$La and $^{146}$Ba are also indicated.

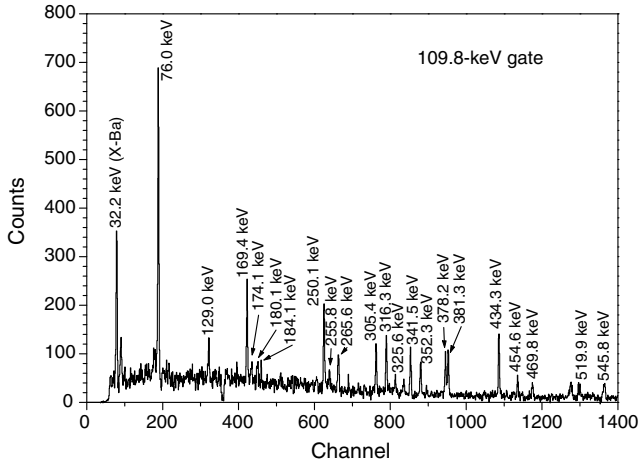


**Fig. 2.** A low-energy portion of the $\gamma$-ray spectrum in coincidence with the 109.8 keV transition selected in the LOAX spectrometer. It represents a sum of the spectra recorded in the 15% and 80% Ge detectors.

the Warsaw-Uppsala-Świerk Collaboration and are complementary to the studies of octupole collective nuclei in the heavy actinide region performed at the ISOLDE facility at CERN (see ref. [11] and references quoted therein).

$^{147}$Ba is the heaviest odd-$A$ Ba nucleus for which excited states are known empirically. The experimental information has been obtained from the $\beta^-$-decay of $^{147}$Cs [12] ($Q_\beta = 8.58(22)$ MeV [13]) and prompt-fission studies performed at the GAMMASPHERE [14] and EUROGAM II [9] arrays. No features related to strong octupole correlations were observed although a number of $E1$ transitions were reported [12] among the low-lying states.

No strong octupole correlations were reported for $^{149}$Ce, which represents the closest experimentally investigated $N = 91$ isotone of $^{147}$Ba. In recent studies of $^{149}$Ce from the $\beta^-$-decay of $^{149}$La [15,16] we have observed pronounced quadrupole deformation which dominated octupole effects. Consequently, the nuclear structure of $^{149}$Ce could be reproduced in the model calculations assuming a reflection-symmetric shape. In comparison to $^{149}$Ce, however, one would expect $^{147}$Ba to exhibit higher octupole and lower quadrupole collectivities.

## 2 Experimental procedure

The experiments were carried out at the fission product mass separator OSIRIS at Studsvik, Sweden [17]. The radioactive beam of mass 147 was produced via thermal neutron-induced fission of $^{235}$U target integrated in an ion source. The mass separated activity was deposited onto an aluminized Mylar tape in the moving-tape collection system.

The $\gamma$-ray singles and then $\gamma$-$\gamma$ coincidences were measured using a three-detector system, which included a low-energy photon and X-ray (LOAX) detector and two high-purity germanium detectors with relative efficiencies of 15% and 80%, respectively. The energy resolutions were 0.6 keV at 81 keV for the LOAX, and 1.8 keV and 2.9 keV at 1.33 MeV for the 15% and 80% Ge detectors, respectively. The detectors were placed in a close geometry at the collection point. The gamma-ray singles spectra were collected in a multispectrum scaling (MSS) mode, where a measurement cycle of 4.8 s was divided into eight time intervals of 0.6 s each. Due to a short half-life of $^{147}$Cs ($T_{1/2} = 0.225$ s [18]) which decays to $^{147}$Ba, the activity was collected during the first time group of the measurement. The beam was then deflected and the source was let decay out during the next seven consecutive time groups. Finally, the tape moved the old activity away and a new cycle was started.

The strongest $\gamma$-rays, which decayed out with the half-life consistent with $T_{1/2} = 0.225$ s, were assigned to the decay of $^{147}$Cs. Their intensities were determined from the $\gamma$-ray singles spectra collected during the first time group of 0.6 s to avoid possible mixing with long-lived impurities. In the case of a few strong $\gamma$-lines in $^{147}$Ba mixed with impurity lines of known intensities, appropriate corrections were made. An example of a $\gamma$-ray singles spectrum collected in the LOAX detector during the first 0.6 s is showed in fig. 1. The $\gamma$-$\gamma$ coincidences served to identify weaker transitions and to construct the decay scheme of $^{147}$Cs to $^{147}$Ba. Since the coincidence measurement aimed also to identify lines from the decays of $^{147}\text{Ba} \rightarrow {}^{147}\text{La} \rightarrow {}^{147}\text{Ce}$, which was very helpful in the analysis of the $^{147}$Ba data, a separate measurement was performed with the length of each group time being set to 3.0 s. The radioactive sample was collected during the first, second and third time groups. Then the beam was deflected and the activity was let decay out for the remaining five time groups.

In the $\gamma$-$\gamma$ analysis of $^{147}$Ba only data from the first three time groups were considered. The assignment of $\gamma$-lines to the $^{147}$Cs decay was based on their decay patterns measured in the MSS spectra, on the $\gamma$-$\gamma$ coincidences and coincidences with the X-rays of Ba. An example of a coincidence spectrum is presented in fig. 2.

**Table 1.** Energies, intensities and placements in the level scheme of $\gamma$ transitions belonging to the $^{147}$Cs $\rightarrow$ $^{147}$Ba decay.

| Transition energy (keV) | $I^{\gamma}_{\rm rel}$ | Initial level (keV) | Final level (keV) | Transition energy (keV) | $I^{\gamma}_{\rm rel}$ | Initial level (keV) | Final level (keV) |
|---|---|---|---|---|---|---|---|
| 24.4(1)$^{(\star)}$ | 16(3)$^{(a)}$ | 109.8 | 85.4 | 426.1(1) | 73(12)$^{(c)}$ | 426.1 | 0.0 |
| 35.2(2) | 12(4)$^{(b)}$ | 327.4 | 292.1 | 434.3(1) | 81(23)$^{(b)}$ | 544.1 | 109.8 |
| 39.2(1)$^{(\star)}$ | 37(4)$^{(b)}$ | 85.4 | 46.2 | 444.8(1) | 182(36)$^{(a)}$ | 491.1 | 46.2 |
| 46.2(1)$^{(\star)}$ | 317(50)$^{(c)}$ | 46.2 | 0.0 | 452.4(1) | 58(5)$^{(b)}$ | 744.4 | 292.1 |
| 76.0(1)$^{(\star)}$ | 121(17)$^{(c)}$ | 185.8 | 109.8 | 454.6(2) | 19(4)$^{(b)}$ | 564.4 | 109.8 |
| 85.4(1)$^{(\star)}$ | 1000(50)$^{(c)}$ | 85.4 | 0.0 | 459.7(1) | 56(9)$^{(a)}$ | 787.1 | 327.4 |
| 100.4(1)$^{(\star)}$ | 37(8)$^{(b)}$ | 185.8 | 85.4 | 462.1(1)$^{(\star)}$ | 424(58)$^{(c)}$ | 462.1 | 0.0 |
| 109.8(1)$^{(\star)}$ | 826(19)$^{(c)}$ | 109.8 | 0.0 | 469.8(3) | 54(5)$^{(c)}$ | 655.6 | 185.8 |
| 116.4(1) | 20(4)$^{(c)}$ | 513.8 | 397.5 | 479.0(1) | 69(7)$^{(a)}$ | 564.4 | 85.4 |
| 123.9(1) | 21(4)$^{(c)}$ | 451.3 | 327.4 | 501.5(5) | 49(8)$^{(b)}$ | 587.0 | 85.4 |
| 129.0(1) | 34(9)$^{(a)}$ | 238.8 | 109.8 | 519.9(2) | 47(10)$^{(a)}$ | 705.7 | 185.8 |
| 134.6(1) | 30(8)$^{(b)}$ | 462.1 | 327.4 | 540.8(1) | 211(31)$^{(a)}$ | 587.0 | 46.2 |
| 139.6(1)$^{(\star)}$ | 31(7)$^{(b)}$ | 185.8 | 46.2 | 545.8(3) | 35(3)$^{(b)}$ | 655.6 | 109.8 |
| 153.4(1) | 26(4)$^{(a)}$ | 238.8 | 85.4 | 549.2(2) | 72(18)$^{(a)}$ | 595.6 | 46.2 |
| 169.4(1) | 68(18)$^{(a)}$ | 279.2 | 109.8 | 557.0(3) | 53(5)$^{(b)}$ | 642.3 | 85.4 |
| 174.1(2)$^{(\star)}$ | 51(9)$^{(b)}$ | 359.9 | 185.8 | 564.3(1) | 54(4)$^{(c)}$ | 564.4 | 0.0 |
| 179.9(2) | 29(8)$^{(b)}$ | 365.6 | 185.8 | 570.3(3) | 40(4)$^{(b)}$ | 655.6 | 85.4 |
| 180.1(2) | 72(7)$^{(c)}$ | 642.3 | 462.1 | 582.1(1) | 193(31)$^{(a)}$ | 628.3 | 46.2 |
| 184.1(2) | 7(2)$^{(b)}$ | 544.1 | 359.9 | 587.0(1) | 141(33)$^{(c)}$ | 587.0 | 0.0 |
| 185.8(1)$^{(\star)}$ | 367(12)$^{(a)}$ | 185.8 | 0.0 | 593.9(1) | 40(4)$^{(a)}$ | 921.2 | 327.4 |
| 186.4(1) | 130(21)$^{(c)}$ | 513.8 | 327.4 | 595.8(1)$^{(\star)}$ | 136(17)$^{(c)}$ | 595.6 | 0.0 |
| 204.4(2) | 10(2)$^{(c)}$ | 564.4 | 359.9 | 601.3(5) | 60(21)$^{(b)}$ | 787.1 | 185.8 |
| 216.8(1) | 25(2)$^{(a)}$ | 544.1 | 327.4 | 609.9(2) | 16(4)$^{(b)}$ | 719.8 | 109.8 |
| 221.7(1)$^{(\star)}$ | 111(18)$^{(c)}$ | 513.8 | 292.1 | 620.3(2) | 30(6)$^{(a)}$ | 705.7 | 85.4 |
| 238.8(1) | 39(6)$^{(a)}$ | 238.8 | 0.0 | 629.0(2) | 47(15)$^{(a)}$ | 921.2 | 292.1 |
| 241.9(2)$^{(\star)}$ | 123(12)$^{(b)}$ | 327.4 | 85.4 | 630.9(1) | 84(6)$^{(a)}$ | 716.3 | 85.4 |
| 245.9(1)$^{(\star)}$ | 865(59)$^{(c)}$ | 292.1 | 46.2 | 634.4(1) | 55(9)$^{(b)}$ | 719.8 | 85.4 |
| 250.1(3)$^{(\star)}$ | 77(20)$^{(b)}$ | 359.9 | 109.8 | 663.8(2) | 19(4)$^{(b)}$ | 773.6 | 109.8 |
| 255.8(1) | 18(5)$^{(a)}$ | 365.6 | 109.8 | 673.6(1) | 33(6)$^{(a)}$ | 719.8 | 46.2 |
| 265.0(1) | 87(17)$^{(c)}$ | 544.1 | 279.2 | 691.9(4) | 21(5)$^{(b)}$ | 801.7 | 109.8 |
| 265.6(2)$^{(\star)}$ | 70(14)$^{(a)}$ | 451.3 | 185.8 | 698.1(2) | 112(11)$^{(b)}$ | 744.4 | 46.2 |
| 280.2(2)$^{(\star)}$ | 65(8)$^{(b)}$ | 365.6 | 85.4 | 701.8(5) | 28(4)$^{(b)}$ | 787.1 | 85.4 |
| 281.2(1) | 195(24)$^{(a)}$ | 327.4 | 46.2 | 718.2(1) | 51(10)$^{(c)}$ | 1045.6 | 327.4 |
| 293.1(1) | 17(8)$^{(b)}$ | 744.4 | 451.3 | 723.9(1) | 21(4)$^{(a)}$ | 1015.9 | 292.1 |
| 294.7(3) | 14(4)$^{(a)}$ | 587.0 | 292.1 | 740.9(2) | 66(5)$^{(a)}$ | 787.1 | 46.2 |
| 303.6(2) | 13(4)$^{(a)}$ | 595.6 | 292.1 | 770.8(4) | 23(4)$^{(c)}$ | 1262.0 | 491.1 |
| 305.4(2)$^{(\star)}$ | 168(9)$^{(b)}$ | 491.1 | 185.8 | 773.6(2) | 34(7)$^{(c)}$ | 773.6 | 0.0 |
| 312.2(1) | 308(30)$^{(c)}$ | 397.5 | 85.4 | 786.8(3) | 25(12)$^{(a)}$ | 1078.9 | 292.1 |
| 316.3(2) | 65(21)$^{(c)}$ | 426.1 | 109.8 | 798.2(3) | 31(10)$^{(a)}$ | 1090.3 | 292.1 |
| 319.4(1)$^{(\star)}$ | 259(15)$^{(b)}$ | 365.6 | 46.2 | 801.7(1) | 79(17)$^{(c)}$ | 801.7 | 0.0 |
| 325.6(3) | 78(8)$^{(c)}$ | 564.4 | 238.8 | 820.7(2) | 21(6)$^{(b)}$ | 930.5 | 109.8 |
| 327.4(2)$^{(\star)}$ | 506(99)$^{(b)}$ | 327.4 | 0.0 | 841.8(3) | 50(5)$^{(a)}$ | 1239.5 | 397.5 |
| 327.8(2)$^{(\star)}$ | 43(12)$^{(b)}$ | 513.8 | 185.8 | 916.7(4) | 23(4)$^{(b)}$ | 1209.0 | 292.1 |
| 336.3(3) | 7(5)$^{(b)}$ | 628.3 | 292.1 | 930.5(1) | 56(17)$^{(a)}$ | 1015.9 | 85.4 |
| 340.7(1)$^{(\star)}$ | 81(3)$^{(b)}$ | 426.1 | 85.4 | 947.5(5) | 25(5)$^{(a)}$ | 1239.5 | 292.1 |
| 341.5(2)$^{(\star)}$ | 51(10)$^{(a)}$ | 451.3 | 109.8 | 969.6(4) | 27(6)$^{(b)}$ | 1262.0 | 292.1 |
| 350.3(2)$^{(\star)}$ | 73(8)$^{(b)}$ | 642.3 | 292.1 | 1015.9(3) | 64(12)$^{(c)}$ | 1015.9 | 0.0 |
| 351.2(1)$^{(\star)}$ | 639(33)$^{(c)}$ | 397.5 | 46.2 | 1045.6(2) | 47(11)$^{(c)}$ | 1045.6 | 0.0 |
| 352.3(1)$^{(\star)}$ | 43(11)$^{(a)}$ | 462.1 | 109.8 | 1140.4(2) | 70(5)$^{(a)}$ | 1326.2 | 185.8 |
| 365.9(1)$^{(\star)}$ | 212(15)$^{(b)}$ | 451.3 | 85.4 | 1176.7(2) | 69(13)$^{(a)}$ | 1262.0 | 85.4 |
| 378.2(1) | 78(8)$^{(b)}$ | 738.1 | 359.9 | 1193.4(2) | 91(14)$^{(a)}$ | 1239.5 | 46.2 |
| 381.3(2)$^{(\star)}$ | 47(10)$^{(a)}$ | 491.1 | 109.8 | 1209.0(2) | 29(8)$^{(c)}$ | 1209.0 | 0.0 |
| 397.4(2)$^{(\star)}$ | 34(9)$^{(c)}$ | 397.5 | 0.0 | 1415.1(3) | 37(5)$^{(a)}$ | 1707.2 | 292.1 |
| 405.8(1)$^{(\star)}$ | 112(10)$^{(b)}$ | 491.1 | 85.4 | 2114.4(8) | 79(17)$^{(b)}$ | 2300.2 | 185.8 |
| 424.3(2) | 14(3)$^{(b)}$ | 716.3 | 292.1 | 2279.8(10) | 46(10)$^{(b)}$ | 2365.2 | 85.4 |

$^{(a)}$ Average value of $\gamma$ intensities taken from $\gamma$-ray singles and $\gamma$-$\gamma$ data.
$^{(b)}$ $\gamma$ intensity deduced from $\gamma$-$\gamma$ data.
$^{(c)}$ $\gamma$ intensity taken from $\gamma$-ray singles spectra.
$^{(\star)}$ $\gamma$-line also observed in the previous $\beta^-$ study [12]; its new energy could be different from the old value by up to $\sim$ 1 keV.

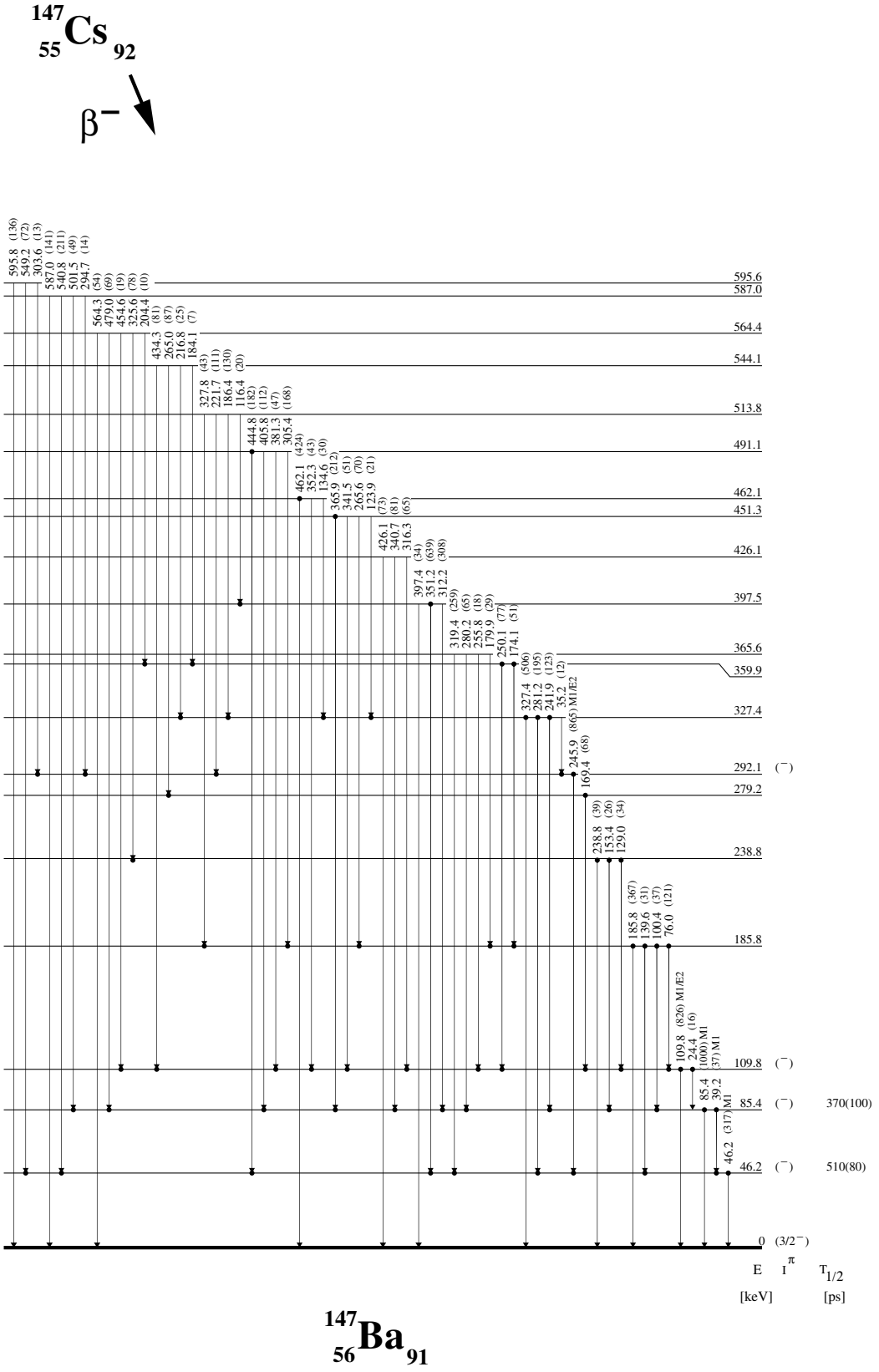


**Fig. 3.** The level scheme of $^{147}$Ba observed in the $\beta^-$-decay of $^{147}$Cs; from this work. The $M1/E2$ multipolarity for the 109.8 keV transition is from [9]. Dots at the ends of arrows were used to mark transitions seen in appropriate coincidence spectra.

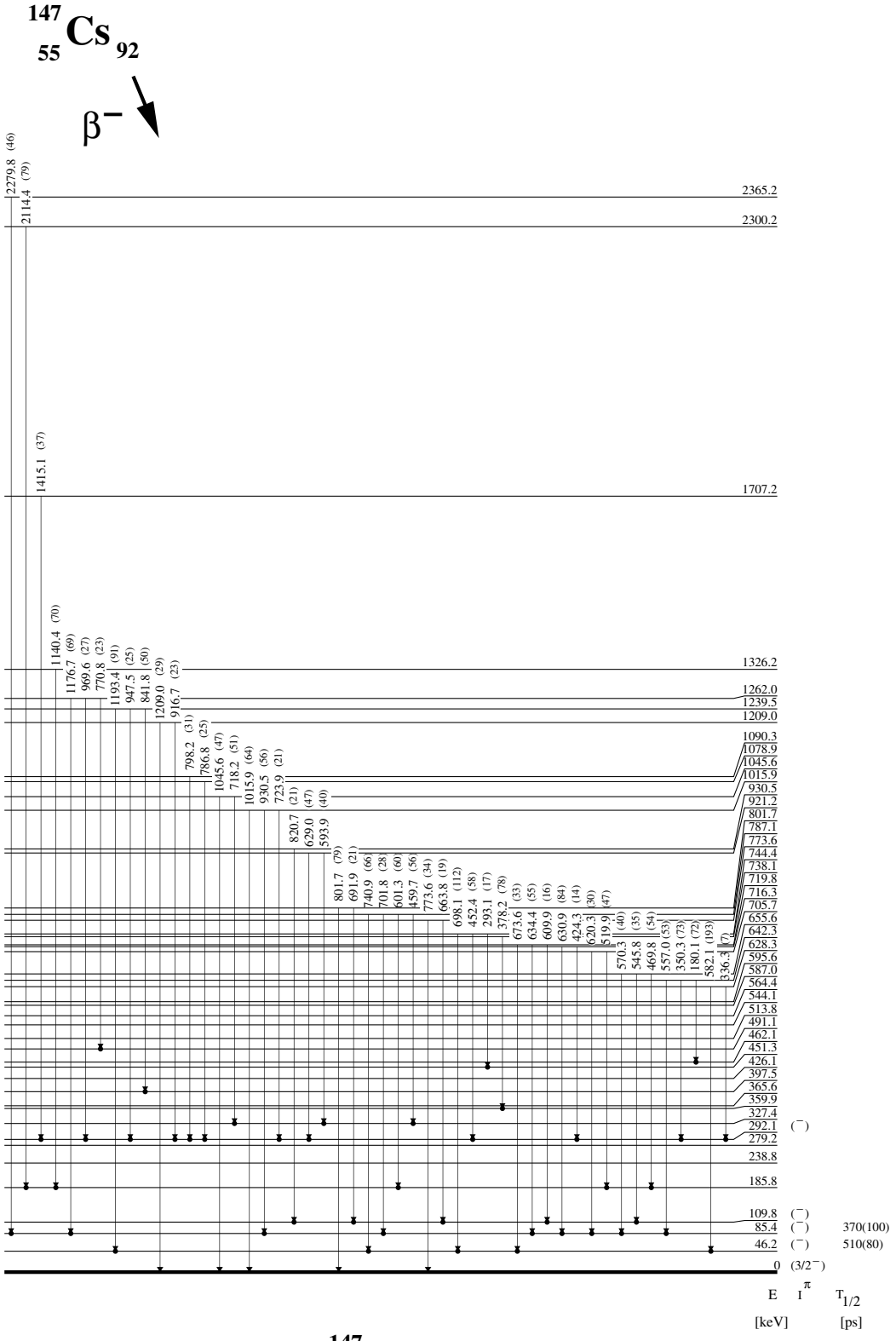


**Fig. 3.** Continued.

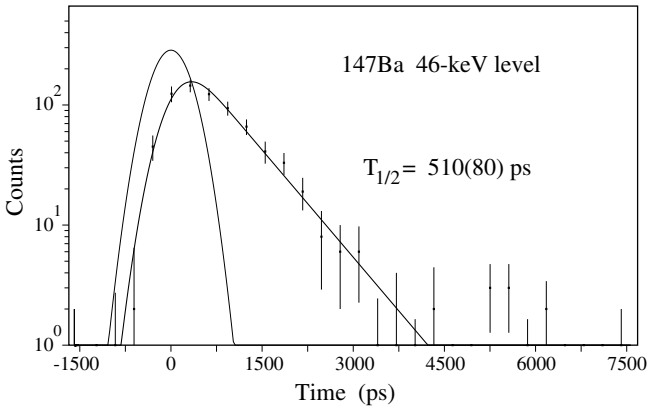


**Fig. 4.** Time-delayed $\beta\gamma\gamma$(t) spectrum showing the decay of the 46.2 keV level. It was obtained by gating on the 245.9 and 351.2 keV $\gamma$ transitions in the Ge and on the 46.2 keV transition in the $BaF_2$ spectra.

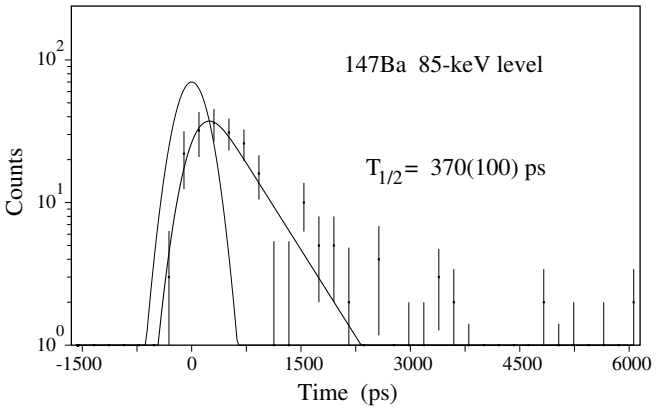


**Fig. 5.** Time-delayed $\beta\gamma\gamma$(t) spectrum showing the decay of the 85.4 keV level. It was obtained by gating on the 312.2 and 405.8 keV $\gamma$ transitions in the Ge and on the 85.4 keV transition in the $BaF_2$ spectra.

The energies and relative intensities of $\gamma$ transitions in $^{147}$Ba, which were corrected for detector efficiencies and normalized to the $\gamma$ intensity of 1000 for the strongest 85.4 keV $\gamma$-ray, are listed in table 1 together with their placement in the level scheme illustrated in fig. 3.

The lifetimes of the excited states in $^{147}$Ba were measured using the Advanced Time-Delayed (ATD) $\beta\gamma\gamma$(t) method [19–21]. The triple-coincidence measurement involved two fast-response scintillators, a small 2.5 cm long $BaF_2$ crystal for $\gamma$-ray and a thin 3 mm thick NE111A plastic for $\beta$ particle detection, respectively. A third coincidence with $\gamma$-rays recorded in a high-purity Ge detector was used to select the desired $\gamma$-ray cascade. The Ge detector had a relative efficiency of about 25% and an energy resolution of 2.1 keV at 1.33 MeV. All detectors were positioned close to the beam deposition point. The thin $\Delta E$ $\beta$ detector provided almost uniform time response to $\beta$-rays of different energies. The information on level lifetime was derived from the analysis of time-delayed $\beta\gamma$(t) spectra recorded in the fast scintillators. A valid $\beta\gamma\gamma$(t) coincidence event started the data acquisition system. The measurement cycle included eight time intervals, each 0.2 s long. The radioactivity was deposited during all eight time groups and then the sample was moved away by the tape system. A standard calibration of the time response of the $BaF_2$ detector was made after the $^{147}$Ba measurement using the mass-separated $^{140}$Ba source [19]. Two half-lives have been measured: $T_{1/2} = 510(80)$ ps for the 46 keV level and $T_{1/2} = 370(100)$ ps for the 85 keV state as illustrated in fig. 4 and fig. 5, respectively. Both results were obtained in the $\chi^2$-minimization–based fitting procedure of the whole spectrum to a response function which was constructed by a convolution of the Gaussian prompt and an exponential decay curve [19]. In the analysis care was taken to ensure that the $\gamma$-rays feeding the levels from above do not de-excite states with long lifetimes that would impact the shape fitting. For example, fig. 4 illustrates the time-delayed $\beta\gamma\gamma$(t) spectrum showing the decay of the 46 keV level. It was obtained by gating on the 246 and 351 keV $\gamma$ transitions in the Ge and on the 46 keV transition in the $BaF_2$ spectra. By inverting the gates, thus by selecting the 46 keV line in Ge and a common gate on the 246 and 351 keV transitions in $BaF_2$, we obtained a time-delayed spectrum which reveals the time components of the feeding $\gamma$ transitions. Since the spectrum had no slope (below 100 ps), the slope fitting of the time spectrum in fig. 4 is not affected by lifetimes of higher-lying levels that are de-excited via the 246 and 351 keV transitions. A similar analysis was done for the cascade feeding the 85 keV level. A more detailed discussion of the fitting procedures can be found in [19].

**Table 2.** Internal conversion coefficients (ICC) for transitions in $^{147}$Ba.

| Energy (keV) | Shell | ICC | | | | Dominant multi-polarity |
|---|---|---|---|---|---|---|
| | | Exp. | Theoretical[a] | | | |
| | | | $E1$ | $E2$ | $M1$ | |
| 46.2 | $K$ | 7.2(8) | 1.58 | 7.82 | 8.02 | $M1$, $E2$, $M1+E2$ |
| 245.9 | all | 0.08(2) | 0.02 | 0.09 | 0.08 | $M1$, $E2$, $M1+E2$ |

([a]) From ref. [22].

## 3 Experimental results and discussion

### 3.1 Level scheme of $^{147}$Ba

The results of this work are summarized in tables 1, 2 and 3, and in fig. 3. A new level scheme for the decay of $^{147}$Cs to $^{147}$Ba is established on the basis of coincidence results and is significantly different from the one previously reported [12]. Fifteen $\gamma$ transitions and four excited levels reported in [12] have not been observed in this work, while 79 new $\gamma$ lines and 29 new excited levels have been found in our study. As an important difference, we note that the $\gamma$-line of 35 keV, which was reported in [12] to

**Table 3.** Level lifetimes and experimental transition probabilities for transitions in $^{147}$Ba.

| $E_{\rm level}$ (keV) | $T_{1/2}$ (ps) | $E_\gamma$ (keV) | $\gamma$-branching (%) | $B^{\rm exp}(M1)$ ($\mu_N^2$) | $B^{\rm exp}(M1)$ (W.u.)[a] | $B^{\rm exp}(E2)$ ($e^2{\rm fm}^4$) | $B^{\rm exp}(E2)$ (W.u.)[b] |
|---|---|---|---|---|---|---|---|
| 46.2 | 510(80) | 46.2 | 9.6 | 0.08(1) | 0.04 | $1.5 \cdot 10^5$ | $3.2 \cdot 10^3$ |
| 85.4 | 370(100) | 39.2 | 1.2[c] | 0.03(1) | 0.02 | $1.7 \cdot 10^5$ | $3.8 \cdot 10^3$ |
| 85.4 | 370(100) | 85.4 | 31.4[d] | 0.05(2) | 0.03 | $6.7 \cdot 10^4$ | $1.4 \cdot 10^3$ |

[a] 1 W.u.= $1.790\,\mu_N^2$ for the $M1$ transition.
[b] 1 W.u.= $5.940 \cdot 10^{-2} A^{4/3}\ e^2{\rm fm}^4$ for the $E2$ transition.
[c] Assuming the 85.4 keV transition to be of $M1$ type.
[d] Assuming the 39.2 keV transition to be of $M1$ type.

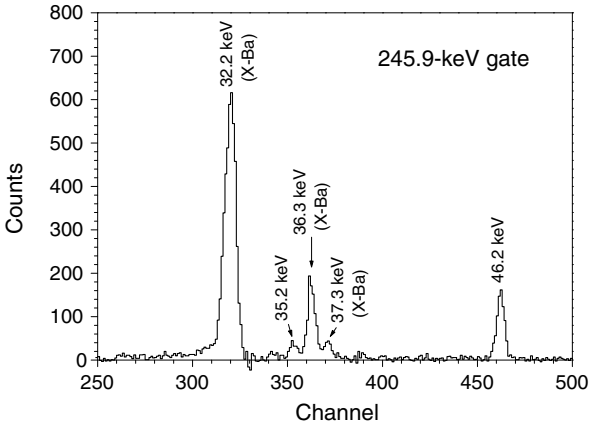


**Fig. 6.** Portion of a $\gamma$-ray spectrum, recorded in LOAX, in coincidence with the 245.8 keV transition selected in the Ge detectors.

de-excite the 110 keV state, was established in this work to de-excite the 327 keV level (see fig. 6 and the decay scheme in fig. 3).

Unfortunately, $\gamma$ lines from the $^{147}$Cs $\rightarrow$ $^{147}$Ba decay were masked by much stronger $\gamma$ transitions from $^{147}$Ba $\rightarrow$ $^{147}$La, and the case was further complicated by multiple placements of a number of $\gamma$-rays in both $^{147}$Ba and $^{147}$La. The $\gamma$-ray intensities determined in this work are mostly in agreement with those reported in [12]. There are a few exceptions, however. For example, the intensity for the 46 keV transition is reported by us to be about two times lower than in ref. [12]. As a possible source of error we note that 46 keV transition was also observed in $^{147}$La as a doublet [18].

The $\beta^-$-decay studies are complementary to the high-spin work and they often allow to correct the low-spin part of a level scheme observed in the latter experiments (see, *e.g.*, [15]). Out of ten excited states in $^{147}$Ba identified in the high-spin study by Jones *et al.* [9], four levels are observed in this work. We note some differences in the relative intensities of $\gamma$-rays de-exciting the 186 and 360 keV levels quoted here and in ref. [9]. For the 360 keV level, which is moderately strongly populated in the $\beta$-decay work, we do not observe the 81 keV line in coincidence with the 169 keV transition in our $\gamma$-$\gamma$ spectra although it would be expected by the results reported in [9]. Moreover, the relative ratio of intensities for the 250 and 174 keV transitions de-exciting the 360 keV level is found in our $\beta$-decay study as 1.5 while in the high-spin work it was about 17. For the 186 and 76 keV transitions depopulating the 186 keV level we report the ratio of 3.0, which is somewhat higher than 1.1 reported in ref. [9].

### 3.2 Multipolarities of low-energy transitions

In the previous $\beta$-decay study of $^{147}$Cs [12,18], most of the reported multipolarities were of $M1$, $E2$ or $M1$+$E2$ character. In ref. [12] $E1$ multipolarity was proposed for the 46 and 199 keV transitions. In the Nuclear Data Sheets for $A = 147$ [18] the compilers list $E1$ multipolarity also for the 35, 39, 64, and 139 keV transitions. On the other hand, in the high-spin work, no $E1$ transitions were identified [9] while the strong 110 keV transition was assigned to be of mixed $M1/E2$ character on the basis of the internal conversion coefficient measurements.

In our work two of the proposed $E1$ $\gamma$-rays, at 64 and 199 keV, have not been found, while the previous $E1$ assignment to the 46 keV line does not agree with our results firmly indicating the $M1$ character of the transition. As a consequence of the new assignment to the 46 keV $\gamma$-ray, the previous results need to be re-evaluated. In particular, the very weak $\gamma$-ray at 39 keV cannot be $E1$ as the multipolarity of the 27 times stronger transition of energy 85 keV measured in the same work [12] as $M1$, is correct. Moreover, the 140 keV transition, depopulating the 186 keV level to the one at 46 keV, cannot be $E1$ as the competing 186 keV transition was measured as $M1/E2$ by Schussler *et al.* [3]. Both, the 140 and 186 keV transitions, feed levels of the same parity, namely the one at 46 keV and the ground state, respectively. We could not confirm the $E1$ parity assignment to the very weak 35 keV transition.

In the present study, multipolarities for the 46 and 246 keV transitions were deduced from the internal conversion coefficients obtained either from eq. (1) or (2) given below. The $K$-conversion coefficient can be deduced from

$$\alpha_K = \frac{I_K}{I_\gamma}\frac{1}{\omega_K}, \qquad (1)$$

where $I_K$ and $I_\gamma$ are the $K_{\alpha+\beta}$ X-rays and $\gamma$-ray intensities, respectively, corrected for detector efficiency, and $\omega_K$ is the fluorescence yield (the fraction of $K$-shell vacancies which decay with the production of X-rays). Alternatively, one can use the intensity balance

$$I_\gamma^1(1+\alpha_{\rm tot}^1) = I_\gamma^2(1+\alpha_{\rm tot}^2), \qquad (2)$$

where $I_\gamma$ are the $\gamma$ intensities of two coincident $\gamma$ transitions numbered as 1 and 2 in a suitable $\gamma$-$\gamma$ coincidence spectrum, while $\alpha_{\rm tot}$ is the conversion coefficient summed over all conversion components. Following eq. (1), the $\alpha_K$ conversion coefficient for the 46 keV line was deduced from a sum of coincidence spectra gated by the 541, 582, 674, 741 and 1193 keV transitions. The summed LOAX spectrum shows coincident 46 keV $\gamma$-line and its associated X-rays of Ba. The deduced $\alpha_K = 7.2(8)$ allows only for $M1$, $E2$ or $M1$+$E2$ multipolarity assignments and clearly excludes the $E1$ character for the 46 keV transition (see table 2). This result is in disagreement with the $E1$ multipolarity proposed in [12].

In the coincidence spectrum gated by the 222 keV transition (see the decay scheme in fig. 3) two $\gamma$ transitions of energies 246 and 46 keV have equal total intensities. Following eq. (2) we obtain $\alpha_{\rm tot} = 0.08(2)$ for the 246 keV $\gamma$-ray by adopting pure $M1$ multipolarity for the 46 keV transition (this is justified based on the lifetime result discussed in the next section). One can exclude $E1$ character of the 246 keV transition as the deduced ICC value is only consistent with $M1$, $E2$ or $M1$+$E2$ multipolarity (see table 2) which does agree with the $M1$+$E2$ assignment proposed in [12].

As discussed below, the lifetime measurements of excited states allowed to establish a dominant $M1$ character for the 46, 39, and 85 keV transitions.

### 3.3 Lifetimes of the 46.2 and 85.4 keV levels

We have measured the half-lives of the 46 and 85 keV states as $T_{1/2} = 510(80)$ ps and 370(100) ps, respectively. The data are presented in figs. 4 and 5. The time-delayed spectrum in the first figure represents a sum of $\beta$-gated spectra involving the 246-46 keV and 351-46 keV $\gamma$-cascades registered in the Ge and $BaF_2$ detectors, respectively, while the spectrum in the second figure represents the sum involving the 312-85 and 406-85 keV cascades. Each lifetime result is an averaged value obtained over a few independent $\chi^2$-fits with different data compressions and/or fitting ranges of the same spectrum.

It is difficult to compare our lifetime results with those reported in ref. [12], since the latter have a preliminary character and no uncertainties in those values have been provided. Moreover, due to the use of the $\beta$-Ge time-delayed coincidences in ref. [12], the gated time spectra for $A = 147$ could represent a mixture of different time components. For example, a time spectrum gated on the 46 keV full energy peak, would likely represent a mixture of time components due to different overlapping 46 keV transitions from $^{147}$Ba and $^{147}$La. In contrast, in our analysis we use triple coincidences and have a freedom to select in the Ge detector those $\gamma$-rays which feed the state from above and do not represent mixed transitions. In any case, it is obvious from very large differences in the half-life values measured in ref. [12] and in this work, that the half-lives of 1.4 ns and 2.1 ns reported in ref. [12] for the 46 and 85 keV states have been affected by significant impurities.

Using the newly measured level lifetimes, we examine the $B(M1)$ and $B(E2)$ rates for the transitions de-exciting the 46 and 85 keV states. The reduced transition probabilities, $B(M1)$ and $B(E2)$, are expressed as functions of the partial mean life $\tau_\gamma$ for a given $\gamma$ transition and its energy, $E_\gamma$, using the standard formulas:

$$B(M1) = 5.68 \cdot 10^{-14} \cdot E_\gamma^{-3} \cdot \tau_\gamma^{-1}\,(\mu_N^2), \qquad (3)$$

and

$$B(E2) = 8.20 \cdot 10^{-10} \cdot E_\gamma^{-5} \cdot \tau_\gamma^{-1}\,(e^2 \cdot {\rm fm}^4), \qquad (4)$$

where $E_\gamma$ and $\tau_\gamma$ are in units of MeV and s, respectively.

The measured half-lives of the 46 and 85 keV levels and the experimental transition probabilities $B$(XL) for $\gamma$ transitions de-exciting those levels are presented in table 3. Assuming a 100% $M1$ or $E2$ character of the 46 keV transition, one obtains $B(M1) = 0.08(1)\ \mu_N^2$ (0.04 W.u.) and $B(E2) \sim 1.5 \cdot 10^5\ e^2{\rm fm}^4$ ($\sim 3000$ W.u.). Since such a large $B(E2)$ is not realistic, it certifies that any $E2$ admixture to this transition is very weak, thus it can be assumed to have an almost pure $M1$ character.

As for the 85 keV level for which the half-life of 370 (100) ps was measured, two low-energy transitions are competing in the de-excitation process, *i.e.* the 39 and 85 keV ones. Similarly to the case of the 46 keV $\gamma$-ray, extraordinary large $B(E2)$ rates ($> 1000$ W.u.) for these $\gamma$-rays certify that the $E2$ character is not possible for either 39 or 85 keV transitions. Assuming that both transitions are $M1$, the obtained $M1$ rates amount to $0.03(1)\ \mu_N^2$ (0.02 W.u.) and $0.05(2)\ \mu_N^2$ (0.03 W.u.) for the 39 and 85 keV transitions, respectively. A very small admixture of $E2$ cannot be excluded.

The $B(M1)$ values deduced in this work, which are of the order of $10^{-2}$ W.u., are of an average $M1$ strength for the $A = 91$–$150$ nuclei as reported by Endt [23].

### 3.4 The ground state of $^{147}$Ba

As of now, the spin and parity of the ground state of $^{147}$Ba remain unknown (a tentative assignment of $3/2^-$ has been proposed in ref. [12]). Below we examine predictions of model calculations.

Recent study of $^{149}$Ce [15] shows that the $3/2^-$ spin and parity assignment to the ground state of this $N = 91$ Ce isotone is consistent with calculations of the Nilsson model and a rotational model including Coriolis coupling and pairing interaction (RQPC) [15] as well as with calculations of pairing correlations in odd cerium isotopes performed by Duguet *et al.* [24] using the Skyrme Hartree-Fock-Bogolubov method. In the adjacent $N = 89$ $^{145}$Ba isotope strong octupole correlations pushed down

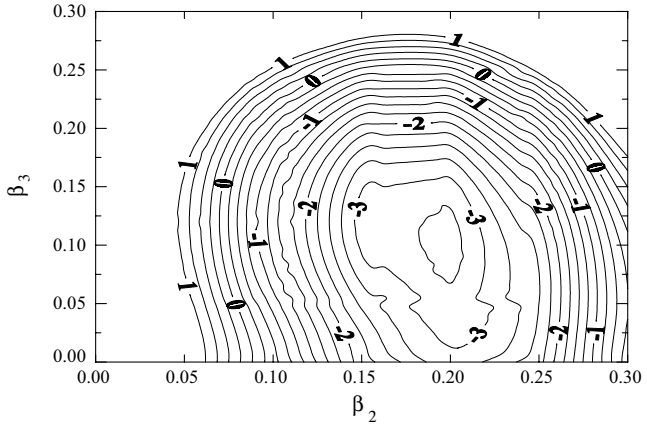


**Fig. 7.** The deformation energy in the $(\beta_2, \beta_3)$-plane for the $\Omega = 3/2$ configuration. The distance between contour lines is equal to 250 keV. Labels of the lines mean energies in MeV.

the $I = 5/2$ $\Omega = 5/2$ orbital due to the interaction of 5/2[532] with 5/2[642] [6]. This parity-mixed orbital has a somewhat larger component of negative parity than positive parity, so the $^{145}$Ba ground state was predicted to be the negative-parity member of the $5/2^{\pm}$ parity doublet. A spin of $I = 5/2$ was assigned to the ground state of $^{145}$Ba by collinear fast-beam laser spectroscopy at ISOLDE [25].

We have calculated the properties of the ground state of $^{147}$Ba using a shell correction approach with an axially deformed Woods-Saxon potential [26,27]. We found three almost degenerated configurations: $I = \Omega = 1/2$, 3/2 and 5/2 with deformation parameters $\beta_2 \simeq 0.18$, $\beta_3 \simeq 0.11$, $\beta_4 \simeq 0.07$. Due to octupole interaction between $\nu i_{13/2}$ and $\nu f_{7/2}$ orbitals, all calculated configurations are parity mixed and the most dominant components are 1/2[660], 3/2[532], and 5/2[642] for $\Omega = 1/2$, 3/2 and 5/2, respectively. For the case of $\Omega = 3/2$, the plot of deformation energy as a function of $\beta_2$ and $\beta_3$ is shown in fig. 7. The shallow minimum for $\Omega = 3/2$ means that the $^{147}$Ba nucleus is less stiff with respect to octupole deformation. More stable reflection-asymmetric deformation is predicted for the $\Omega = 1/2$ and 5/2 configurations.

No firm assignment of spin and parity to the ground state of $^{147}$Ba can be deduced either from our experimental results or theoretical calculations discussed above. We propose a very tentative assignment of $I = 3/2^-$, which was also suggested in ref. [12].

## 4 Summary

The nucleus of $^{147}$Ba has been investigated by means of $\gamma$- and X-ray spectroscopy and fast-timing $\beta\gamma\gamma$(t) method. It is the most exotic odd-$A$ Ba nucleus for which excited states are known experimentally. The levels in $^{147}$Ba were populated in the $\beta^-$-decay of $^{147}$Cs produced at the OSIRIS fission product mass separator at Studsvik. A significantly modified level scheme of $^{147}$Ba has been determined and extended up to an excitation energy of 2365 keV. On the basis of the internal conversion coefficient analysis, the $E1$ character of 46 keV transition has been excluded, and the $M1$ multipolarity with a possible $E2$ admixture was determined for the 46, 85 and 246 keV transitions. The half-lives of the low-lying levels at 46 and 85 keV were measured as 510(80) and 370(100) ps, respectively, using the Advanced Time-Delayed $\beta\gamma\gamma$(t) method. The $B(M1)$ values obtained for the 39, 46 and 85 keV transitions range from 0.017 to 0.043 W.u. and represent typical $B(M1)$ strengths in the Ba-Er region. Theoretical calculations performed using the shell correction approach with the axially deformed Woods-Saxon potential predict for the ground state of $^{147}$Ba an octupole deformation with deformation parameter $\beta_3 = 0.11$. Three almost degenerated configurations $\Omega = 1/2$, 3/2 and 5/2 correspond to the minimum binding energy of the nucleus.

The authors would like to thank the former NORDBALL collaboration for the use of the Ge spectrometers. One of the authors (A.S.) is grateful to the OSIRIS group for the hospitality during her visits to Studsvik. This work was supported in part by the Swedish-Polish Scientific Exchange Programme and the Swedish Research Council. Theoretical calculations were partially supported by the Polish State Committee for Scientific Research (KBN) grant No. 1 P03B 059 27. An access to the facility at the Studsvik Neutron Research Laboratory has been supported by the European Community-Access to Research Infrastructure action of the Improving Human Potential Programme, contract No. HPRI-CT 1999-00061.

## References

1. W. Nazarewicz, P. Olanders, I. Ragnarsson, J. Dudek, G.A. Leander, P. Möller, E. Ruchowska, Nucl. Phys. A **429**, 269 (1984).
2. W.R. Phillips, I. Ahmad, H. Emling, R. Holzmann, R.V.F. Janssens, T.-L. Khoo, M.W. Drigert, Phys. Rev. Lett. **57**, 3257 (1986).
3. P. Schüler, Ch. Lauterbach, Y.K. Agarwal, J. De Boer, K.P. Blume, P.A. Butler, K. Euler, Ch. Fleischmann, C. Gunther, E. Hauber, H.J. Maier, M. Marten-Tolle, Ch. Schandera, R.S. Simon, R. Tolle, P. Zeyen, Phys. Lett. B **174**, 241 (1986).
4. H. Mach, W. Nazarewicz, D. Kusnezov, M. Moszyński, B. Fogelberg, M. Hellström, L. Spanier, R.L. Gill, R.F. Casten, A. Wolf, Phys. Rev. C **41**, R2469 (1990).
5. P.A. Butler, W. Nazarewicz, Nucl. Phys. A **533**, 249 (1991).
6. G.A. Leander, W. Nazarewicz, P. Olanders, I. Ragnarsson, J. Dudek, Phys. Lett. B **152**, 284 (1985).
7. S. Ćwiok, W. Nazarewicz, Nucl. Phys. A **496**, 367 (1989).
8. S.J. Zhu, Q.H. Lu, J.H. Hamilton, A.V. Ramayya, L.K. Peker, M.G. Wang, W.C. Ma, B.R.S. Babu, T.N. Ginter, J. Kormicki, D. Shi, J.K. Deng, W. Nazarewicz, J.O. Rasmussen, M.A. Stoyer, S.Y. Chu, K.E. Gregorich, M.F. Mohar, S. Asztalos, S.G. Prussin, J.D. Cole, R. Aryaeinejad, Y.K. Dardenne, M. Drigert, K.J. Moody, R.W. Lougheed, J.F. Wild, N.R. Johnson, I.Y. Lee, F.K. McGowan, G.M. Ter-Akopian, Yu.Ts. Oganessian, Phys. Lett. B **357**, 273 (1995).

9. M.A. Jones, W. Urban, J.L. Durell, M. Leddy, W.R. Phillips, A.G. Smith, B.J. Varley, I. Ahmad, L.R. Morss, M. Bentaleb, E. Lubkiewicz, N. Schulz, Nucl. Phys. A **605**, 133 (1996).
10. W. Urban, T. Rząca-Urban, J.L. Durell, W.R. Phillips, A.G. Smith, B.J. Varley, N. Schulz, I. Ahmad, Phys. Rev. C **69**, 017305 (2004).
11. W. Kurcewicz, Hyperfine Interact. **129**, 175 (2000).
12. F. Schussler, B. Pfeiffer, H. Lawin, E. Monnand, J. Münzel, J.A. Pinston, K. Sistemisch, *Proceedings of the 4th International Conference on Nuclei Far from Stability, Helsingør, Denmark, 1981*, CERN Report 81-09, edited by P.G. Hansen, O.B. Nielsen (1981) p. 589.
13. G. Audi, O. Bersillon, J. Blachot, A.H. Wapstra, Nucl. Phys. A **729**, 3 (2003).
14. B.R.S. Babu, S.J. Zhu, A.V. Ramayya, J.H. Hamilton, L.K. Peker, M.G. Wang, T.N. Ginter, J. Kormicki, W.C. Ma, J.D. Cole, R. Aryaeinejad, K. Butler-Moore, Y.X. Dardenne, M.W. Drigert, G.M. Ter-Akopian, Yu.Ts. Oganessian, J.O. Rasmussen, S. Asztalos, I.Y. Lee, A.O. Macchiavelli, S.Y. Chu, K.E. Gregorich, M.F. Mohar, S. Prussin, M.A. Stoyer, R.W. Lougheed, K.J. Moody, J.F. Wild, Phys. Rev. C **54**, 568 (1996).
15. A. Syntfeld, H. Mach, R. Kaczarowski, W. Kurcewicz, W. Płóciennik, W. Urban, B. Fogelberg, P. Hoff, Nucl. Phys. A **710**, 221 (2002).
16. A. Syntfeld, H. Mach, W. Kurcewicz, B. Fogelberg, W. Płóciennik, E. Ruchowska, Phys. Rev. C **68**, 024304 (2003).
17. B. Fogelberg, M. Hellström, L. Jacobsson, D. Jerrestam, L. Spanier, G. Rudstam, Nucl. Instrum. Methods B **70**, 137 (1992).
18. E. der Mateosian, L.K. Peker, Nucl. Data Sheets **66**, 705 (1992).
19. H. Mach, R.L. Gill, M. Moszyński, Nucl. Instrum. Methods Phys. Res. A **280**, 49 (1989).
20. M. Moszyński, H. Mach, Nucl. Instrum. Methods Phys. Res. A **277**, 407 (1989).
21. H. Mach, F.K. Wohn, G. Molnar, K. Sistemich, J.C. Hill, M. Moszyński, R.L. Gill, W. Krips, D.S. Brenner, Nucl. Phys. A **523**, 197 (1991).
22. R.S. Hager, E.C. Seltzer, Nucl. Data A **4**, 1 (1968).
23. P.M. Endt, At. Data Nucl. Data Tables **26**, 47 (1981).
24. T. Duguet, P. Bonche, P.-H. Heenen, J. Meyer, Phys. Rev. C **65**, 014310 (2002).
25. A.C. Mueller, F. Buchinger, W. Klempt, E.W. Otten, R. Neugart, C. Ekstrom, J. Heinemeier, Nucl. Phys. A **403**, 234 (1983).
26. S. Ćwiok, J. Dudek, W. Nazarewicz, J. Skalski, T. Werner, Comput. Phys. Commun. **46**, 379 (1987).
27. R. Bengtsson, J. Dudek, W. Nazarewicz, P. Olanders, Phys. Scr. **39**, 196 (1989).